

Hierarchy of gaps and magnetic minibands in graphene in the presence of the Abrikosov vortex lattice

Xi Chen and Vladimir I. Fal'ko

National Graphene Institute, University of Manchester, Booth Street East, Manchester M13 9PL, United Kingdom

(Received 11 July 2015; revised manuscript received 13 December 2015; published 15 January 2016)

We determine the bands and gaps in graphene subjected to the magnetic field of an Abrikosov lattice of vortices in the underlying superconducting film. The spectrum features one nondispersive magnetic miniband at zero energy, separated by the largest gaps in the miniband spectrum from a pair of minibands resembling a slightly broadened first Landau level in graphene, suggesting the persistence of $v = \pm 2$ and ± 6 quantum Hall effect states. Also, we identify an occasional merging point of magnetic minibands with a Dirac-type dispersion at the miniband edges.

DOI: 10.1103/PhysRevB.93.035427

Studies of superlattices in two-dimensional (2D) electron systems recently have been boosted by the development of van der Waals heterostructures of graphene with hexagonal boron nitride (hBN). In such systems, the superlattice effects, observed in scanning tunneling microscopy (STM) spectra [1–3], magnetotransport characteristics [4–6], and quantum capacitance [7], are produced by a periodic moiré pattern, with the period a determined by a slight incommensurability and misalignment between graphene and hBN crystals [1,8,9] and reflect the formation of superlattice minibands for graphene's Dirac electrons [4,7,9]. To a large extent, the possibility to observe the superlattice effects in graphene-hBN heterostructures owes to the high mobility of electrons in such systems, where graphene is encapsulated between hBN sheets both protecting from contamination and permitting to vary the electrons' density over a broad range using electrostatic gates. When subjected to a strong external magnetic field, the superlattice leads to the formation of a "Hofstadter butterfly," a sparse spectrum of minibands [10–12] formed at magnetic field values corresponding to the magnetic flux $\Phi = \frac{p}{q}\phi_0$ (through the area $S = \sqrt{3}a^2/2$ of the superlattice unit cell) commensurate with the flux quantum $\phi_0 = h/e$.

Here, we consider a magnetic superlattice [13–18] that can be realized in a ballistic hBN-graphene-hBN stack by placing it over a high- H_{c2} superconductor film (e.g., Nb, W, or MoRe alloys). In such a system, where no alignment control of graphene and hBN lattices is required, the long-range periodic structure is caused by the Abrikosov lattice of vortices [19,20] formed in a superconductor subjected to an external magnetic field $H < H_{c2}$, sketched in the inset of Fig. 1. In contrast to the earlier theories developed for spatially alternating magnetic fields with a zero average [21–26], the Abrikosov lattice produces magnetic induction with a spatial average $B = \phi_0/(\sqrt{3}a^2)$ linked to the magnetic lattice period a . As each vortex carries the flux $h/2e$, the vortex lattice realizes the simplest fundamental fraction $\frac{p}{q} = \frac{1}{2}$ in the Brown-Zak commensurability condition for a magnetic field flux in a 2D periodic system [10,11].

Figure 1 shows the hierarchy of bands and gaps in the corresponding spectrum of Dirac electrons calculated in this work and plotted as a function of $4\pi\lambda^2 B/\phi_0$. The latter parameter characterizes the ratio between the lattice period $a = \sqrt{\phi_0/\sqrt{3}B}$ and the penetration depth λ in a superconductor.

The spectrum in Fig. 1 features one degenerate magnetic miniband which precisely coincides with the zero-energy $m = 0$ Landau level (LL) that is peculiar for Dirac electrons, and two other low-energy bands which resemble slightly broadened $m = \pm 1$ LLs. At the same time, the higher-energy minibands (traceable at $4\pi\lambda^2 B/\phi_0 \geq 1$ to LLs with $|m| \geq 1$ at $E = \frac{m}{|m|}v\sqrt{2|m|\hbar eB}, m \in \mathbb{Z}$) are strongly broadened, and they overlap on the energy scale when $a \gg \lambda$, forming Dirac-type features at conjoint miniband edges.

The distribution of the magnetic field of Abrikosov's lattice (for isotropic superconductors, the vortex lattice is hexagonal) is given by [19,20]

$$H(\mathbf{r}) = \sum_{\mathbf{R}_i} H_v(\mathbf{r} - \mathbf{R}_i), \quad H_v(\mathbf{r}) = \frac{1}{2\pi} \frac{\phi_0}{2\lambda^2} K_0\left(\frac{r}{\lambda}\right),$$

where \mathbf{R}_i picks the location of each individual vortex with the field profile given by the modified Bessel function of the imaginary argument, with $K_0(x \ll 1) \approx \ln \frac{1}{x}$ and $K_0(x \gg 1) \approx \sqrt{\frac{\pi}{2x}} e^{-x}$. For convenience, we use a Fourier representation for the periodic field of the vortex lattice [20] and the corresponding vector potential,

$$\begin{aligned} H(\mathbf{r}) &= B \left(1 + \sum_{\mathbf{g}_{n_1 n_2}} \frac{1}{1 + \lambda^2 g_{n_1 n_2}^2} e^{-i\mathbf{g}_{n_1 n_2} \cdot \mathbf{r}} \right), \\ \mathbf{A} &= \bar{\mathbf{A}} - \frac{\hbar\sqrt{3}}{e 8\pi} \sum_{n_1 n_2} \frac{\hat{\mathbf{l}}_z \times \nabla e^{-i\mathbf{g}_{n_1 n_2} \cdot \mathbf{r}}}{\omega_{n_1 n_2}^2 (1 + \alpha^2 \omega_{n_1 n_2}^2)}, \\ (\nabla \times \bar{\mathbf{A}})_z &= B \equiv \frac{h/e}{\sqrt{3}a^2}, \quad \alpha \equiv \frac{\sqrt{3}a}{4\pi\lambda}, \end{aligned} \quad (1)$$

and a nonorthogonal coordinate system adjusted to the hexagonal symmetry of the vortex superlattice,

$$\begin{aligned} \mathbf{g}_{n_1 n_2} &= g\hat{\mathbf{z}} \times (n_1 \hat{\mathbf{x}}_1 + n_2 \hat{\mathbf{x}}_2), \\ \omega_{n_1 n_2} &= \sqrt{n_1^2 + n_2^2 + n_1 n_2}, \quad g = 4\pi/(\sqrt{3}a), \\ \hat{\mathbf{x}}_1 &= \frac{1}{2}\hat{\mathbf{x}} + \frac{\sqrt{3}}{2}\hat{\mathbf{y}}, \quad \hat{\mathbf{x}}_2 = -\frac{1}{2}\hat{\mathbf{x}} + \frac{\sqrt{3}}{2}\hat{\mathbf{y}}. \end{aligned}$$

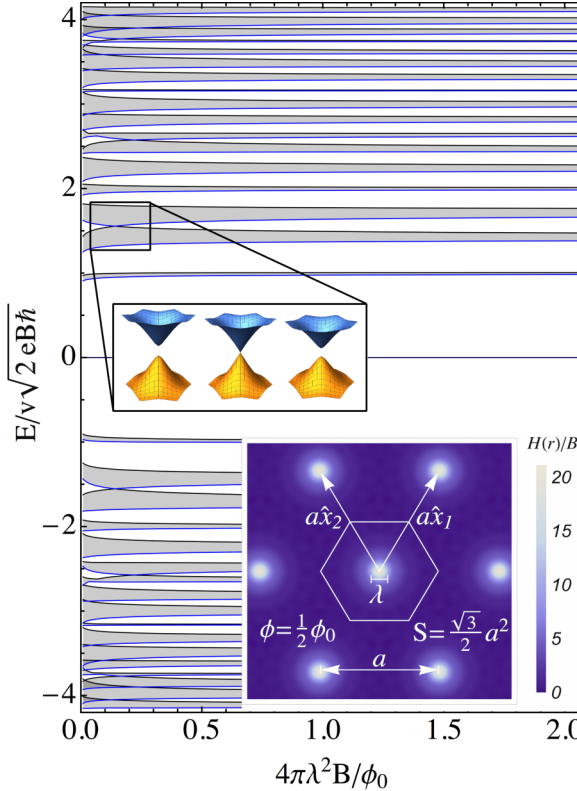


FIG. 1. Spectrum of Dirac electrons in graphene in a magnetic field of an Abrikosov vortex lattice, with one degenerate band at $E = 0$. Energy is scaled as $v\sqrt{2\hbar eB} \equiv \frac{2}{3^{1/4}} v\sqrt{\pi}/a$, and the magnetic field as $4\pi\lambda^2 B/\phi_0$. Inset: Second and third miniband dispersions over the folded magnetic Brillouin minizone near their touching condition.

The spectrum of electrons in the K and K' valleys of graphene is determined by the Hamiltonian

$$\mathcal{H} = v\boldsymbol{\sigma} \cdot (\boldsymbol{p} - e\tilde{\boldsymbol{A}})$$

$$+ \hbar v \boldsymbol{\sigma} \cdot \frac{\sqrt{3}}{8\pi} \sum_{n_1 n_2} \frac{\hat{\boldsymbol{l}}_z \times \nabla e^{-i\mathbf{g}_{n_1 n_2} \cdot \mathbf{r}}}{\omega_{n_1 n_2}^2 (1 + \alpha^2 \omega_{n_1 n_2}^2)}, \quad (2)$$

where $\tilde{\boldsymbol{A}} = \hbar x_1(-\hat{x}_1 + 2\hat{x}_2)/(3a^2e)$, $x_1 = x + \frac{1}{\sqrt{3}}y$, $x_2 = -x + \frac{1}{\sqrt{3}}y$, and $v \approx 10^6$ cm/s is the Dirac velocity in graphene. This Hamiltonian acts in the space of two-component wave functions describing the electrons' amplitudes on the A and B sublattices of the honeycomb lattice of carbons, with the basis choice $[\Psi(A), \Psi(B)]$ in valley K and $[\Psi(B), -\Psi(A)]$ in valley K' : This choice provides us with the same form of the Hamiltonian in both valleys.

To find the magnetic miniband spectrum corresponding to Hamiltonian (2), we use [12] the basis of Bloch states (with $s = -N/2, \dots, N/2$, and $t = 0, 1$),

$$|_t^m(\mathbf{k})\rangle = \frac{1}{\sqrt{N}} \sum_s e^{-i2sk_1 a} \psi_m^{k_2 + \frac{\sqrt{3}}{4}g(2s+t)}, \quad (3)$$

$$k_1 = \frac{1}{2}k_x + \frac{\sqrt{3}}{2}k_y, \quad k_2 = -\frac{1}{2}k_x + \frac{\sqrt{3}}{2}k_y,$$

built of LL states ψ_m , $E_m = \frac{m}{|m|} \frac{\hbar v}{a} \sqrt{\frac{\pi}{\sqrt{3}} |m|}$ ($m \in \mathbb{Z}$) of Dirac electrons in a homogeneous magnetic field B [27]:

$$\psi_0^{k_2} = \frac{e^{ik_2 x_2}}{\sqrt{L}} \begin{pmatrix} \varphi_0 \\ 0 \end{pmatrix}, \quad \psi_{m \neq 0}^{k_2} = \frac{e^{ik_2 x_2}}{\sqrt{2L}} \begin{pmatrix} \varphi_{|m|} \\ \frac{m}{|m|} e^{i\frac{\pi}{3}} \varphi_{|m|-1} \end{pmatrix},$$

$$\varphi_n = C_n \left(\frac{2\pi}{\sqrt{3}a^2} \right)^{1/4} e^{-\frac{1}{2}z_{k_2}^2(1+\frac{i}{\sqrt{3}})} \mathbb{H}_n(z_{k_2}), \quad (4)$$

$$C_n = \sqrt{\frac{3}{\sqrt{\pi} 2^{(n+1)} n!}}, \quad z_{k_2} = \frac{3^{1/4}}{\sqrt{2\pi}} \left(\frac{\pi}{a} x_1 + k_2 a \right).$$

Here, \mathbb{H}_m are Hermite polynomials, and the sign of m identifies the conduction ($m > 0$) and valence ($m < 0$) band states.

The states in the basis set $|_t^m(\mathbf{k})\rangle$ transform according to the irreducible representations of the symmetry group \mathcal{M}_6^2 of the vortex lattice field, which includes C_6 rotations and magnetic translations $\mathcal{G} = \{\hat{\Theta}_X = e^{i\pi n'_1 x_2/a} \hat{T}_X, X = n'_1 a\hat{x}_1 + n'_2 a\hat{x}_2\} \subset \mathcal{M}_6^2$. In contrast to usual translations, magnetic translations do not commute with each other, $\Theta_{a_1} \Theta_{a_2} = -\Theta_{a_2} \Theta_{a_1}$, however, the group \mathcal{M}_6^2 contains an Abelian subgroup,

$$\mathcal{G}' = \{\hat{\Theta}_R = e^{i\pi n'_1 x_2/a} \hat{T}_R, R = 2n'_1 a\hat{x}_1 + 2n'_2 a\hat{x}_2\},$$

which is formed by translations on a superlattice with an isotropically doubled period and a unit cell area $4S$. Because of this, it is possible to classify the states on the magnetic superlattice using the wave vector \mathbf{q} taken over the folded Brillouin zone (BZ) with the area $\frac{\sqrt{3}}{8} g^2$, four times smaller than the BZ area of the geometrical vortex lattice. Each of these folded states is twofold degenerate [10,12], which is prescribed by the anticommutation, $\Theta_{a_1} \Theta_{a_2} = -\Theta_{a_2} \Theta_{a_1}$, of the operators of elementary translations. By analyzing the characters of the magnetic translation group \mathcal{M}_6^2 , one can find that the latter features six different two-dimensional irreducible representations related to the states with the wave vector $\mathbf{q} = \mathbf{0}$ in the center of magnetic BZ. In practice, these six types of irreducible representations can be constructed using linear combinations of Bloch functions $|_t^{\pm(6M+N)}(\mathbf{k})\rangle$ with different $M \geq 0$ but fixed $N = 0, 1, 2, 3, 4, 5$.

Using the basis of Bloch functions in Eq. (3), Hamiltonian Eq. (2) can be represented in the form of the Heisenberg matrix,

$$\langle_t^m(\mathbf{k}) | \mathcal{H} | \tilde{\mathbf{k}} \rangle = \frac{\hbar v}{a} \sqrt{\frac{4\pi}{\sqrt{3}}} \delta_{t,\tilde{t}} \delta_{\mathbf{k},\tilde{\mathbf{k}}} \left[\frac{m}{|m|} \sqrt{|m|} \delta_{m,\tilde{m}} + \sum_{n_1 n_2} \frac{e^{-i2n_1 k_1 a}}{\sqrt{(1+\delta_{m0})(1+\delta_{\tilde{m}0})}} \frac{\mu_{m,\tilde{m},n_1,n_2}^{k_2 + \frac{\sqrt{3}}{4}gt, k_2 + \frac{\sqrt{3}}{4}g(n_1+t)}}{\omega_{n_1 n_2}^2 (1 + \omega_{n_1 n_2}^2 \alpha^2)} \right],$$

$$\mu_{m,\tilde{m},n_1,n_2}^{\kappa,\tilde{\kappa}} = \frac{m}{|m|} (n_1 e^{i\pi/3} + n_2) \mathcal{V}_{|m|-1,|\tilde{m}|}(n_2, \kappa, \tilde{\kappa}) - \frac{\tilde{m}}{|\tilde{m}|} (n_1 e^{-i\pi/3} + n_2) \mathcal{V}_{|m|,|\tilde{m}|-1}(n_2, \kappa, \tilde{\kappa}),$$

$$\mathcal{V}_{N,\tilde{N}}(n_2, \kappa, \tilde{\kappa}) = \frac{1}{\sqrt{6}} C_N C_{\tilde{N}} \int_{-\infty}^{\infty} \frac{dx_1}{a} \mathbb{H}_N(z_\kappa) \mathbb{H}_{\tilde{N}}(z_{\tilde{\kappa}}) e^{-\frac{1}{2}z_\kappa^2(1-\frac{i}{\sqrt{3}})} e^{-\frac{1}{2}z_{\tilde{\kappa}}^2(1+\frac{i}{\sqrt{3}})} e^{i\frac{\sqrt{3}}{2}n_2 x_1 g},$$

where $z_\kappa = \frac{3^{1/4}}{\sqrt{2\pi}} (\frac{\pi}{a} x_1 + \kappa a)$.

In Fig. 1, we show bands (shaded) and gaps (white intervals) in the spectrum obtained by numerical diagonalization of the Heisenberg matrix (5). In this calculation we used 80 LLs to guarantee the convergence of the energies in the lowest 20 bands on the conduction and valence band sides, and we included all points $\mathbf{g}_{n_1 n_2}$ in the reciprocal space such that $|\mathbf{g}_{n_1 n_2}| \leq 64\pi/(\sqrt{3}a)$. The calculated energies are scaled with $v\sqrt{2\hbar eB} \equiv \frac{\sqrt{4\pi}}{3^{1/4}} \hbar v/a$ (energy of $|m| = 1$ LL in a homogeneous field B), and they are shown for various values of $4\pi\lambda^2 B/\phi_0$, the parameter we use to characterize the magnetic field distribution across the unit cell. The band diagram in Fig. 1 is electron-hole symmetric, and the hierarchy of bands and gaps in this spectrum is universal, as it can be applied to Dirac electrons in the field of a vortex lattice in a film of any isotropic type-II superconductor. To mention, due to the large demagnetization factor of a film, vortices enter the film at a field much lower than the nominal first critical field of a bulk superconductor, hence justifying the regime of $4\pi\lambda^2 B/\phi_0 \ll 1$. We have set the upper side of the interval of $4\pi\lambda^2 B/\phi_0 \leq 2$ shown in Fig. 1 at the lowest possible limit for the second critical field H_{c2} , knowing that at higher values of $4\pi\lambda^2 B/\phi_0$ the minibands would converge further towards the LL spectrum in a homogenous magnetic field.

The spectrum in Fig. 1 features a dispersionless zero-energy band that exactly coincides with $m = 0$ LL in graphene, both by its energy, large gaps separating it from the rest of the spectrum, and capacity to accommodate electrons. Also, the first magnetic minibands, both on the conduction and valence band side, are only slightly narrowed and follow almost exactly the energy of $m = \pm 1$ LL. All the other magnetic minibands progressively broaden upon the increase of parameter α , and some touch at certain values of α . Such band degeneracies occur due to occasional nonavoided crossings of $\mathbf{q} = \mathbf{0}$ energy levels at the mini-BZ center (γ point). These occasional crossings are allowed by symmetry, because the energy levels ϵ_m^γ at the mini-BZ center belong to one of six different irreducible representations, so that the closest levels do not necessarily “repel” each other on the energy axis.

As different irreducible representations are built by mixing parent LL states which are, at least, $|\delta m| = 6$ apart, such

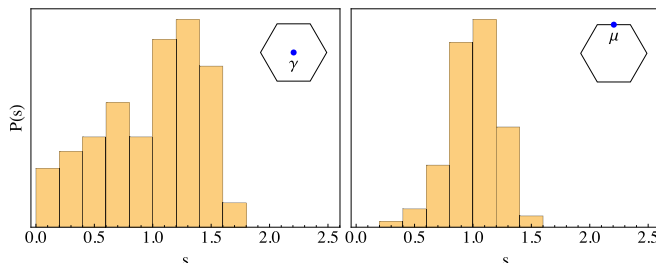


FIG. 2. Distribution function $P(s)$ of the normalized level spacings in the miniband energies at γ and μ points of the Broilouin minizone. Energy levels were taken from more than 30 states sampled ($E = 0$ and the first band excluded) for ten values of $0.5 \leq \alpha \leq 1.5$, with a step of $\delta\alpha = 0.1$.

crossings can be identified by analyzing only the diagonal entries in the Heisenberg matrix (5),

$$\epsilon_m^\gamma = \frac{m}{|m|} \frac{\sqrt{4\pi}}{3^{1/4}} \frac{\hbar v}{a} \sqrt{|m|} \left[1 - \frac{1}{2} \sum_{n_1, n_2} \frac{e^{-\frac{1}{2}t_{n_1, n_2}}}{(1 + \alpha^{-2}\omega_{n_1 n_2}^2)} \times {}_1F_1(1 - |m|, 2, t_{n_1, n_2}) \right],$$

$$t_{n_1, n_2} = \frac{4\pi\omega_{n_1 n_2}^2}{\sqrt{3}},$$

where ${}_1F_1$ is Kummer’s confluent hypergeometric function. Hence, we estimate that, within the interval $\alpha \leq 2$, such crossings would appear at $\alpha_{2,3} = 0.98$ for bands 2 and 3, at $\alpha_{6,7} = 0.90$ for bands 6 and 7, and $\alpha_{14,15} = 1.03$ for bands 14 and 15, and these values are close to the band touching points found in the exact diagonalization of Eq. (5). At a finite \mathbf{q} , such separation of the spectrum into six independent groups is no longer possible.

The separation versus mixing of the groups of levels can be followed for the states at $q \ll \pi/a$ near the γ point, where off-diagonal matrix elements between the closest energy states

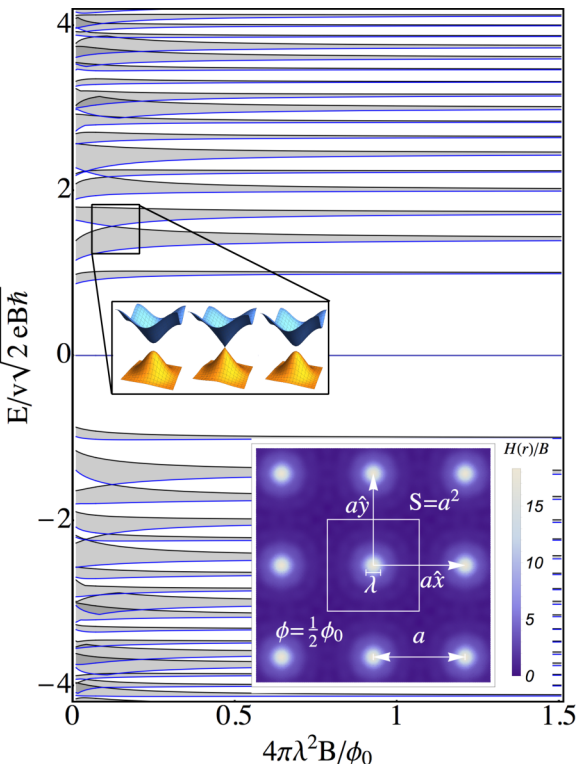


FIG. 3. Spectrum of Dirac electrons in the presence of a square vortex lattice. Energy is scaled by $v\sqrt{2\hbar eB}$, and the spectrum includes one degenerate band at $E = 0$. Inset: Second and third miniband dispersions over the folded magnetic Brillouin zone in the vicinity of their touching condition.

can evaluated analytically [28], leading to a 2×2 matrix,

$$\mathcal{H}_{m+1,m} = \begin{pmatrix} \epsilon_{m+1}^\gamma & \tilde{v}\tau_m(q_x + iq_y \frac{m}{|m|}) \\ \tilde{v}\tau_m^*(q_x - iq_y \frac{m}{|m|}) & \epsilon_m^\gamma \end{pmatrix},$$

$$\tilde{v}_m = \frac{v}{4} \sum_{n_1 n_2} \frac{e^{-\frac{1}{2}t_{n_1 n_2}}}{1 + \alpha^{-2}\omega_{n_1 n_2}^2} \left[L_{|m| + \frac{m}{2|m|} - \frac{1}{2}}^0(t_{n_1 n_2}) \right. \\ \left. - \frac{t_{n_1 n_2}}{\sqrt{(|m| + \frac{m}{2|m|})^2 - 1/4}} L_{|m| + \frac{m}{2|m|} - \frac{3}{2}}^2(t_{n_1 n_2}) \right],$$

where $\tau_m = e^{i\frac{\pi}{6}(3-\frac{m}{|m|})}$ and $L_n^\alpha(x)$ are Laguerre polynomials ($m \neq 0, \pm 1$). This matrix catches the Dirac-type edges of touching bands at $\alpha = \alpha_{m,m+1}$, confirmed by the numerically calculated dispersions plotted over the entire magnetic BZ in the inset of Fig. 1. Note that the velocity of all these “second generation” Dirac electrons appears to be almost the same, $\tilde{v}_{m,m+1} \approx 0.75v$, and, due to the spin and valley degeneracy which has to be factored additionally to the twofold degeneracy of states in magnetic minibands at $\phi = \frac{1}{2}\phi_0$, each of the calculated orbital states in the folded magnetic BZ is eightfold degenerate.

The mixing versus separation of subsets of states in the magnetic minibands can also be traced using the distribution function $P(s)$ of the normalized level spacings (Fig. 2) for

two given points in the Brillouin minizone. For the μ point, it shows a strong “level repulsion” characteristic for the unitary symmetry class of random matrix theory [30]. For the γ point, levels can appear close to each other, as happens in other periodic systems [31–34] where high lattice symmetry splits the spectrum into subsets of states corresponding to different irreducible representations of the lattice symmetry group which can appear arbitrarily close to each other [35–39].

The features we found for the Dirac electrons in hBN-encapsulated graphene placed over a hexagonal Abrikosov vortex lattice suggest that the quantum Hall effect at the filling factors $\nu = \pm 2$ and, to some extent, $\nu = \pm 6$ would remain a robust feature in the transport and capacitance measurements, whereas Shoubnikov–de Haas oscillations at higher filling factors would be strongly suppressed. This property of Dirac electrons in graphene seems to be generic for a broad range of magnetic field distributions. To stress this point, in Fig. 3 we show the calculated spectrum of Dirac electrons moving in a square vortex lattice, which has all the same characteristic features as the spectrum corresponding to the hexagonal vortex lattice.

We thank I. Aleiner, A. K. Geim, I. Grigorieva, and S. Kubatkin for useful discussions. This work was funded by the European Graphene Flagship Project CNECT-ICT-604391, Royal Society, and ERC (Belgium) Synergy Grant Hetero2D.

-
- [1] J. Xue, J. Sanchez-Yamagishi, D. Bulmash, P. Jacquod, A. Deshpande, K. Watanabe, T. Taniguchi, P. Jarillo-Herrero, and B. J. LeRoy, *Nat. Mater.* **10**, 282 (2011).
- [2] R. Decker, Y. Wang, V. W. Brar, W. Regan, H.-Z. Tsai, Q. Wu, W. Gannett, A. Zettl, and M. F. Crommie, *Nano Lett.* **11**, 2291 (2011).
- [3] M. Yankowitz, J. Xue, D. Cormode, J. D. Sanchez-Yamagishi, K. Watanabe, T. Taniguchi, P. Jarillo-Herrero, P. Jacquod, and B. J. LeRoy, *Nat. Phys.* **8**, 382 (2012).
- [4] L. A. Ponomarenko, R. V. Gorbachev, G. L. Yu, D. C. Elias, R. Jalil, A. A. Patel, A. Mishchenko, A. S. Mayorov, C. R. Woods, J. R. Wallbank, M. Mucha-Kruczynski, B. A. Piot, M. Potemski, I. V. Grigorieva, K. S. Novoselov, F. Guinea, V. Fal’ko, and A. K. Geim, *Nature (London)* **497**, 594 (2013).
- [5] C. R. Dean, L. Wang, P. Maher, C. Forsythe, F. Ghahari, Y. Gao, J. Katoch, M. Ishigami, P. Moon, M. Koshino, T. Taniguchi, K. Watanabe, K. L. Shepard, J. Hone, and P. Kim, *Nature (London)* **497**, 598 (2013).
- [6] B. Hunt, J. D. Sanchez-Yamagishi, A. F. Young, M. Yankowitz, B. J. LeRoy, K. Watanabe, T. Taniguchi, P. Moon, M. Koshino, P. Jarillo-Herrero, and R. C. Ashoori, *Science* **340**, 1427 (2013).
- [7] G. Yu, R. Gorbachev, J. Tu, A. Kretinin, Y. Cao, R. Jalil, F. Withers, L. Ponomarenko, B. Piot, M. Potemski, D. Elias, X. Chen, K. Watanabe, T. Taniguchi, I. Grigorieva, K. Novoselov, V. I. Fal’ko, A. Geim, and A. Mishchenko, *Nat. Phys.* **10**, 525 (2014).
- [8] M. Kindermann, B. Uchoa, and D. L. Miller, *Phys. Rev. B* **86**, 115415 (2012).
- [9] J. R. Wallbank, A. A. Patel, M. Mucha-Kruczynski, A. K. Geim, and V. I. Fal’ko, *Phys. Rev. B* **87**, 245408 (2013).
- [10] J. Zak, *Phys. Rev.* **134**, A1602 (1964); **134**, A1607 (1964).
- [11] E. Brown, *Phys. Rev.* **133**, A1038 (1964).
- [12] X. Chen, J. R. Wallbank, A. A. Patel, M. Mucha-Kruczynski, E. McCann, and V. I. Fal’ko, *Phys. Rev. B* **89**, 075401 (2014).
- [13] S. J. Bending, K. von Klitzing, and K. Ploog, *Phys. Rev. Lett.* **65**, 1060 (1990).
- [14] S. J. Bending, K. von Klitzing, and K. Ploog, *Phys. Rev. B* **42**, 9859 (1990).
- [15] G. H. Kruithof, P. C. van Son, and T. M. Klapwijk, *Phys. Rev. Lett.* **67**, 2725 (1991).
- [16] A. K. Geim, *JETP Letters* **50**, 389 (1989); A. K. Geim, S. V. Dubonos, and A. V. Khaetskii, *ibid.* **51**, 121 (1990).
- [17] A. K. Geim, S. J. Bending, and I. V. Grigorieva, *Phys. Rev. Lett.* **69**, 2252 (1992).
- [18] A. K. Geim, V. I. Fal’ko, S. V. Dubonos, and I. V. Grigorieva, *Solid State Commun.* **82**, 831 (1992).
- [19] A. A. Abrikosov, Sov. Phys. JETP-USSR **5**, 1174 (1957); *J. Phys. Chem. Solids* **2**, 199 (1957).
- [20] J. B. Ketterson and S. N. Song, *Superconductivity* (Cambridge University Press, Cambridge, U.K., 1999).
- [21] M. Taillefumier, V. K. Dugaev, B. Canals, C. Lacroix, and P. Bruno, *Phys. Rev. B* **78**, 155330 (2008).
- [22] I. Snyman, *Phys. Rev. B* **80**, 054303 (2009).
- [23] F. Guinea and T. Low, *Philos. Trans. R. Soc. A* **368**, 5391 (2010).
- [24] M. Taillefumier, V. K. Dugaev, B. Canals, C. Lacroix, and P. Bruno, *Phys. Rev. B* **84**, 085427 (2011).
- [25] M. Kamfor, S. Dusuel, K. P. Schmidt, and J. Vidal, *Phys. Rev. B* **84**, 153404 (2011).

- [26] X. Lin, H. Wang, H. Pan, and H. Xu, *Phys. Lett. A* **376**, 584 (2012).
- [27] In the nonorthogonal coordinates we use here, the free-electron Dirac Hamiltonian in a magnetic field has the form ($\lambda_B = \sqrt{\hbar/|eB|} = a\sqrt{\sqrt{3}/(2\pi)}(\begin{smallmatrix} 0 & \hat{d}^\dagger \\ \hat{d} & 0 \end{smallmatrix})$), $\hat{d} = \frac{-2}{\sqrt{3}}[e^{i\frac{2\pi}{3}}\partial_{x_1} + e^{-i\frac{2\pi}{3}}(\partial_{x_2} + i\pi\frac{x_1}{a^2})]$.
- [28] We simplified Eq. (2) using the identity [29] $\int_{-\infty}^{\infty} e^{-x^2} \mathbb{H}_n(x+y) \mathbb{H}_m(x+z) dx = 2^n \sqrt{\pi m!} y^{n-m} L_m^{n-m}(-2yz), n \geq m$.
- [29] A. Jeffrey and D. Zwillinger, *Table of Integrals, Series, and Products* (Academic, New York, 2007).
- [30] M. L. Mehta, *Random Matrices* (Elsevier/Academic, Amsterdam, 2004).
- [31] E. R. Mucciolo, R. B. Capaz, B. L. Altshuler, and J. D. Joannopoulos, *Phys. Rev. B* **50**, 8245 (1994).
- [32] H. Silberbauer, P. Rotter, U. Rössler, and M. Suhre, *Europhys. Lett.* **31**, 393 (1995).
- [33] O. Steffens, M. Suhre, and P. Rotter, *Phys. Rev. B* **55**, 4486 (1997).
- [34] T. Dittrich, B. Mehlig, H. Schanz, and U. Smilansky, *Phys. Rev. E* **57**, 359 (1998).
- [35] G. Fagas, V. I. Fal'ko, C. J. Lambert, and Y. Gefen, *Phys. Rev. B* **61**, 9851 (2000).
- [36] G. Luna-Acosta, J. Méndez-Bermúdez, and F. Izrailev, *Phys. Rev. E* **64**, 036206 (2001).
- [37] L. N. Gumen, J. Arriaga, and A. A. Krokhin, *Physica E* **13**, 459 (2002).
- [38] M. Martínez-Mares and E. Castaño, *Phys. Rev. E* **71**, 036201 (2005).
- [39] G. S. Matharoo and S. K. Sarkar, *Phys. Rev. B* **74**, 144203 (2006).